General and variable features of varicosity spacing along unmyelinated axons in the hippocampus and cerebellum

Gordon M. G. Shepherd*, Morten Raastad, and Per Andersen

Department of Physiology, University of Oslo, Post Box 1103 Blindern, 0317 Oslo, Norway

Contributed by Per Andersen, March 13, 2002

Along unmyelinated central axons, synapses occur at focal swellings called axonal varicosities (boutons). The mechanisms regulating how frequently synapses and varicosities occur along axons remain poorly understood. Here, to investigate varicosity distribution patterns and the extent to which they may be conserved across different axons, we analyzed varicosity numbers and positions along fluorescently labeled axon branches in hippocampal area CA1 (CA3-to-CA1 ''Schaffer collateral'' axons) and five other synaptic regions of rat hippocampus and cerebellum. Varicosity spacing varied by region; e.g., 3.7 ± 0.6 μm (mean ± SD) for CA3-to-CA1 axons and 5.2 ± 1.0 μm for cerebellar parallel fibers. Surprisingly, when 56 axons from these different regions were pooled into a single heterogeneous group, a general relationship emerged: the spacing variability (SD) was a constant fraction of the mean spacing, suggesting that varicosities along different axons are distributed in a fundamentally similar, scaled manner. Varicosity spacing was neither regular nor random but followed a pattern consistent with random synaptic distributions and the occurrence of multiple-synapse boutons. A quantitative model reproduced the salient features of the data and distinguished between two proposed mechanisms relating axonal morphogenesis and synaptogenesis.

Arborizing varicose axons in the central nervous system are complex circuit elements: a single hippocampal CA3 cell axon makes ≈50,000 synapses over ≈0.2 m, all within the hippocampus (1, 2). Understanding connectivity in specific circuits requires detailed quantitative information about axonal synaptic distributions. At the ultrastructural level, synaptic boutons have been characterized as ≈1-μm long (3–5) varicosities that usually occur *en passant* along the axon, separated from other varicosities by short axonal shaft segments. For CA3-to-CA1 and other axons, the average synapse/varicosity ratio is 1.1–1.7 (4–11), reflecting the occurrence of multiple-synapse boutons (MSBs). MSBs may serve as intermediate or final stages of morphological plasticity associated with long-term synaptic plasticity (12–17).

The organization of varicosities and their synapses over longer axonal distances merits quantification for several reasons. First, varicosity spacing is a key aspect of the complex geometry of axon–dendrite interactions. Second, synaptic and varicosity distribution patterns likely reflect fundamental connectivity rules. The report by Hellwig *et al.* (18) of a purely random pattern along neocortical axons carries numerous implications but has not yet been extended to other axon types. Third, varicosity spacing patterns may hold clues about mechanisms of synaptogenesis and development, an unexplored possibility relevant for synaptic plasticity models invoking varicosity neogenesis (15, 16, 19). Here, we used the strategy of quantifying varicosity spacing and its variability at the single axonal branch level for diverse types of central varicose axons, focusing on hippocampal CA3-to-CA1 axons and cerebellar parallel fibers but also including hippocampal axons in more heterogeneous populations to enable comparisons across a variety of axons.

Materials and Methods

Labeling. Adult male and female Wistar rats were anesthetized and killed following institutional animal care guidelines. Hippocampal and cerebellar slices (400 μm) were incubated at room temperature in saline containing: 124 mM NaCl , 2 mM KCl, 2 mM $CaCl_2$, 2 mM $MgSO_4$, 1.25 mM KH_2PO_4, 26 mM $NaHCO_3$, and 22 mM glucose, aerated with 95% O_2-5% CO_2. Slices were transferred briefly to a submersion chamber for labeling, and DiI or DiA (Molecular Probes) was applied to axons either by (*i*) filling pipette tips with subpicoliter volumes of the oily (FAST) forms of the dyes, fracturing the tip against the chamber floor, and depositing the oil-filled shard superficially in the slice; or (*ii*) inserting dye-coated pipettes into slices for 3–6 min (20). Labeled slices were incubated 3–6 h and fixed with 4% paraformaldehyde.

Axon health was controlled for in similarly prepared slices: (*i*) axons generated robust compound action potentials (arrow in Fig. 1*i Inset*) and synaptic field potentials (n = 25 slices); (*ii*) extracellularly stimulated axons, identified visually by patching CA3 cells with pipettes filled with Alexa-488 (Molecular Probes), faithfully conducted trains of action potentials back to the soma (Fig. 1*i*; n = 3 cells); and (*iii*) labeled axons imaged repeatedly for several hours showed no detectable morphological deterioration (n = 3 axons). In addition, we screened all fixed slices, only analyzing regions whose spiny dendrites and other structures appeared healthy (Fig. 1*h*).

Imaging. Fixed samples were rinsed, coverslipped in buffer, and imaged with a confocal scanning laser microscope equipped with a ×60, 1.2-numerical aperture water immersion objective lens. Voxels were 155 × 155 × 486 nm. Sections were scanned twice and averaged. Image stacks comprised up to 100 sections. Most images were taken at slice depths of 50–100 μm, where tissue and optical properties were optimally balanced. Axons were analyzed in three dimensions in stacks by using IGL TRACE (J. C. Fiala and K. M. Harris; freely available at www.synapses.bu.edu). Axons were selected on the basis of favorable imaging characteristics, including high signal-to-noise ratio, labeling over long distances, and lack of overlapping axons, and without regard to particular morphological features. A single exception was an axon in CA1 radiatum with noticeably infrequent varicosities; because of the (intentional) selection bias this axon was excluded from intergroup comparisons, but included in pooled interval and window analyses because they would be unaffected by this type of bias.

Image contrast was set to maintain a wide dynamic range; for most images little or no adjustment was needed. Varicosities

Abbreviations: CV, coefficient of variation; MSB, multiple-synapse bouton; PF, parallel fiber; LM, lacunosum–moleculare; MF, mossy fibers.

*To whom reprint requests should be addressed at the present address: Cold Spring Harbor Laboratory, Marks Building, 1 Bungtown Road, Cold Spring Harbor, NY 11724. E-mail: shepherd@cshl.org.

The publication costs of this article were defrayed in part by page charge payment. This article must therefore be hereby marked "*advertisement*" in accordance with 18 U.S.C. §1734 solely to indicate this fact.

www.pnas.org/cgi/doi/10.1073/pnas.052151299

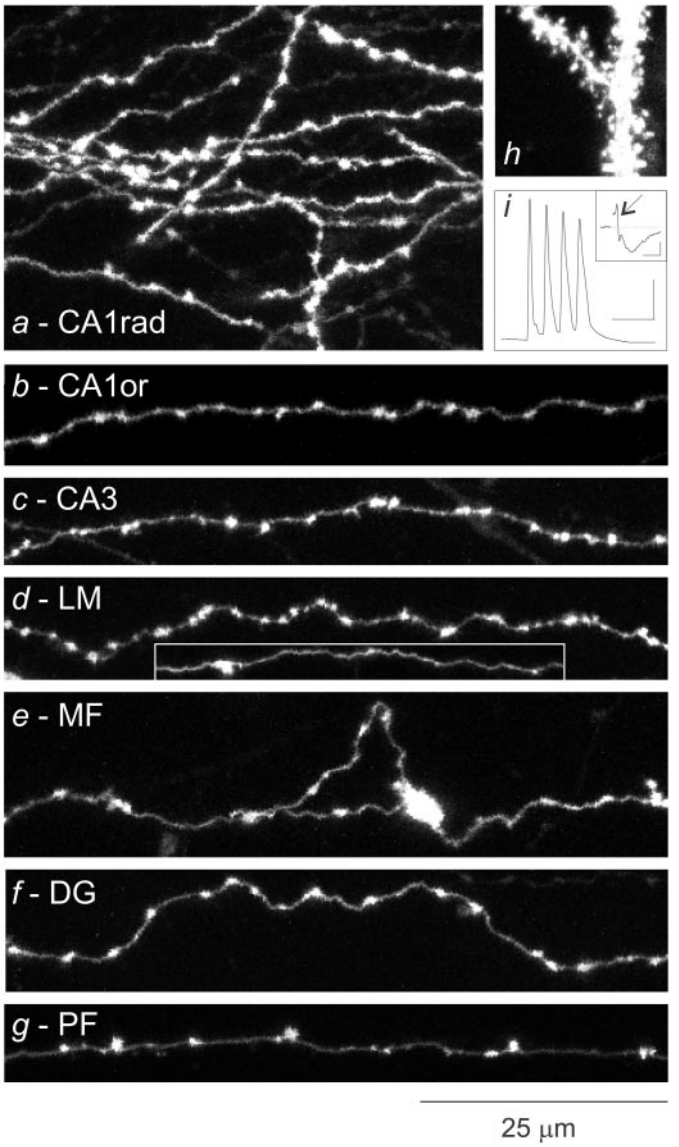

Fig. 1. Morphological features of varicose axons in different synaptic regions. (*A*--*G*) Collapsed views of axons from a variety of synaptic layers in the hippocampus and cerebellum. (*H*) Spiny dendrites from area CA1. (*I*) Train of four action potentials, elicited in the axon and antidromically propagated to and intracellularly recorded at the soma; *Inset* shows compound action potentials (arrow) followed by synaptic potentials, recorded extracellularly. Bars = 25 msec, 25 mV; *Inset*, 2.5 msec, 0.25 mV.

were identified in two stages by using criteria based on the key features of varicose axons. First, we identified all focal swellings that appeared larger and brighter than the adjacent stretches of bare axon. The aim in this initial stage was to apply a low selection threshold because ultrastructural studies have shown that the diameters of smaller varicosities can be only slightly greater than that of the axon; we did not use a more stringent but arbitrary threshold such as a twofold focal increase in diameter. Suspected varicosities were then confirmed as such if they proved evident in the adjacent out-of-plane images (because of their relative brightness and the microscope's point spread function) and more intense than a standard threshold level of 160 on a 0–255 gray scale. The latter was assessed with a software tool that also outlined confirmed varicosities with a contour. Detection of varicosities was accurate and reliable: measurements did not vary with slice depth or axonal distance; observer-dependent variability in counting varicosities was low (estimated at $<5\%$); and results agreed closely with previous ultrastructural measurements (4, 5). Varicosity spacing was measured by calculating the varicosity contour centroids, using these to define varicosity midpoints in x–y–z coordinates, and obtaining the intervaricosity intervals as the center-to-center distances between adjacent midpoints. Correction for out-of-plane axon trajectories was unnecessary because axons were analyzed in three dimensions, as was correction for shrinkage because samples were not dehydrated.

Statistical Analyses. Varicosity positions were analyzed statistically as linear series of distance events (18, 21). Varicosities were treated as equal because (*i*) it is unclear how to translate varicosity size into synaptic weight, because size correlates generally but not precisely with the numbers and dimensions of presynaptic components (e.g., refs. 5–7 and 10) and the average synapse/varicosity ratio is in any case fairly reliable; and (*ii*), most importantly, the spacing of varicosities was independent of their size: when directly measured along a long axon in CA1, the lengths of varicosities and their adjacent shafts showed very low correlation ($n = 101$, Pearson's $r = 0.08$). Varicosity number variability was measured by window analysis. Along individual axons, the numbers of varicosities within consecutive, nonoverlapping windows were counted, providing sets of measurements whose variance/mean ratio gave the index of dispersion. Indices were obtained for window lengths ranging from 2 to at least 30 μm (lengths were increased by 20% per step up to one-sixth of the total length of each particular axon). For each window size, average indices across all axons were also calculated. Clustering was further assessed as follows. For each axon, we first determined the maximal varicosity count, N_{max}, in moving windows, then constructed 1,000 simulated axons with intervals identical to the originals in value but random in sequence and measured N_{max} along these, and then determined how often the simulated N_{max} was equal to or greater than the original N_{max}. This frequency gave an estimate for the probability, P_{orig}, that N_{max} appeared if the intervals were randomly distributed. The expectation for P_{orig} would, however, depend on the number and distribution of varicosities, so we repeated the simulation starting with shuffled intervals to obtain the probability, P_{sim}, that N_{max} would occur in the shuffled distributions. Running these simulations for 56 axons and eight window sizes gave distributions for P_{orig} and P_{sim} that could be compared by using binomial statistics.

Modeling. Nascent synaptic sites were placed at randomly selected points along axons. Varicosities with a length of 1.0 μm were centered over synaptic sites. In the varicosity fusion model, if two synaptic sites were x μm closer than the varicosity length, their varicosities simply overlapped, fusing into a two-synapse varicosity measuring $1.0 + x$ μm in length. Higher numbers of too-close synapses were similarly incorporated in multiple-synapse varicosities (i.e., MSBs). Varicosities' center positions were determined; these matched the synaptic positions for single-synapse varicosities, but differed for MSBs. Another model, the varicosity fission model, also took as a starting point axons with randomly distributed synapses, but too-close synapses were slid apart by increasing their separation to the 1.0 μm varicosity length (reducing all MSBs to single-synapse varicosities). Both models were used to generate 56 axons, each 500 μm long, with mean intervals reflecting the original data. Spatial resolution was 10 nm. Modeled synaptic and varicosity distributions were statistically characterized by the same methods used with the experimental data.

Results

Focal labeling in specific synaptic layers in hippocampal and cerebellar slices gave bright fluorescent labeling of axons and dendrites (Fig. 1 *a–g*). Axonal varicosities varied somewhat in shape and size, most appearing 0.5–2.0 μm in length except for the larger mossy fiber terminals (Fig. 1*e*). Axonal shaft segments appeared isodiametric. Varicosity spacing was clearly variable. In this study we focus on this parameter, which could be measured robustly from fluorescence images (see *Imaging*) and do not explore others such as varicosity sizes except to note a lack of correlation between varicosity length and spacing (see *Statistical Analyses*). We imaged varicosities and analyzed their spacing in six synaptic regions: (*i*) strata radiatum and oriens of area **CA1** (Fig. 1 *a–b*; n = 1,909 varicosities, 27 axons), enriched in CA3 cell axons (CA3-to-CA1, Schaffer/commissural axons); (*ii*) radiatum-oriens of area **CA3** (Fig. 1*c*; n = 232 varicosities, five axons), containing mainly CA3 cell (''associational'') axons; (*iii*) stratum lacunosum–moleculare (**LM**) of area CA1 (Fig. 1*d*; n = 154 varicosities, four axons), containing afferent axons from entorhinal cortex; (*iv*) stratum lucidum of area CA3 (Fig. 1*e*; n = 148 varicosities, four axons), containing dentate granule cell axons (i.e., mossy fibers, **MF**); (*v*) molecular layer (middle and outer) of the dentate gyrus (**DG**; Fig. 1*f*; n = 351 varicosities, seven axons), containing entorhinal cortical (perforant path) axons; and (*vi*) molecular layer of cerebellar cortex (Fig. 1*g*; n = 365 varicosities, nine axons), containing cerebellar granule cell axons (i.e., parallel fibers, **PF**). Interneuronal axons potentially occurred in all these groups. However, we sampled greatest numbers of CA3-to-CA1 and PF axons because these occur in relatively enriched and well-studied populations (3–5), and their identification was frequently aided by their characteristic trajectories (e.g., crossing the CA3/CA1 boundary for radiatum/oriens fibers, and ''T'' shaped and ''parallel'' for PFs). Definitive identification of axon type was otherwise only possible for MFs with characteristic large terminals. The DG and LM samples were thus likely the most heterogeneous because of a variety of glutamatergic and GABAergic axons. Although we evaluated fewer of their axons, their inclusion was nevertheless important because varicosity spacing heterogeneity across all axons formed the basis of the interval and windows analyses (see below).

All unmyelinated axons were varicose, including MFs throughout their length (22, 23) and the ascending limbs of PFs (9). Individual axons often appeared to have distinct mean varicosity densities (e.g., axons in CA1, Fig. 1 *a* and *b* vs. PF, Fig. 1*g*), and in some regions, particularly CA1, mean spacing appeared similar among axons (Fig. 1 *a* and *b*). Axons seemed straight on the scale examined here (average axon length = 225 μm, range 98–495 μm). To quantify this, we arbitrarily selected 12 fibers and compared the path length along the axon (L_p) to the geometric distance between the ends of the axon (L_g). The ratio, L_p/L_g, was 1.06 $\pm$ 0.02 (mean $\pm$ SD, mean L_p = 169 μm), confirming that these short axon branches were virtually straight. Varicosity spacing was assessed by transforming the three-dimensional positions of varicosities along axons into one-dimensional trains of distance events (Fig. 2) (18). Because axons were straight, their linear representations closely matched the original structures.

Mean varicosity spacing, calculated for each axon from its total length and varicosity count, ranged from 2.6 to 9.9 μm (average 4.3 μm). We assessed regional differences by averaging the mean spacing of axons in each region (Fig. 3) (excluding one unusual CA1 radiatum axon; see *Materials and Methods*). Average spacing for the six regions differed significantly (P = 0.001, ANOVA). Closest spacing occurred in CA1 (i.e., CA3-to-CA1 axons), averaging 3.7 $\pm$ 0.6 μm (SD). Parallel fibers also had a narrow range but higher mean (5.2 $\pm$ 1.0 μm). Axons in CA3 (4.2 $\pm$ 1.0 μm) and DG (3.9 $\pm$ 1.4 μm) resembled those in CA1, and MFs (5.1 $\pm$ 1.1 μm) resembled PFs. Axons in CA3 and in CA1, both originating from CA3 cells, did not differ significantly ($P > 0.05$, t test). Low axon-to-axon variability was evident for axons in CA1 (coefficient of variation, CV = 0.16) and PFs (CV = 0.19).

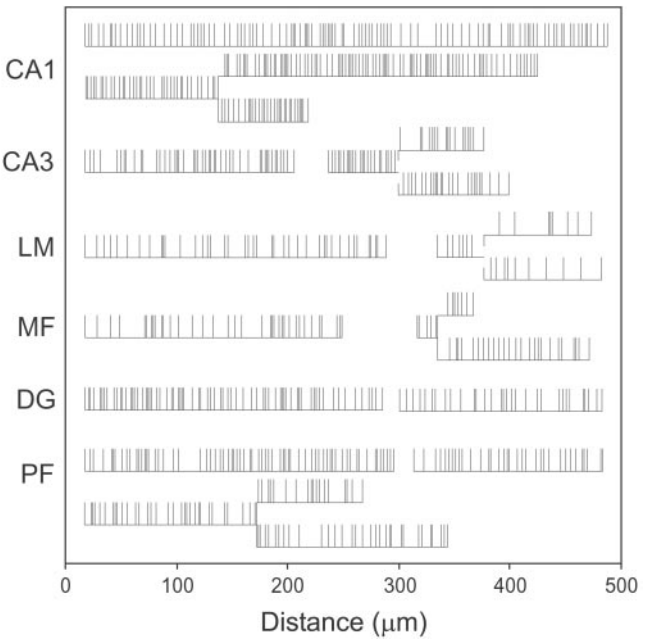

Fig. 2. Examples of linearly transformed axons from each synaptic region, illustrating the variability in varicosity numbers and positions. Vertical lines indicate varicosities. Small vertical gaps at two of the branch points indicate branching that occurred along a bare axon (i.e., not at a varicosity).

Are features of varicosity distribution patterns conserved across different types of axons? We pooled 56 axons from these six regions into one set. Interval analysis of this heterogeneous group revealed two consistent features (Fig. 4 *Inset*). One, an initial gap from 0 to 1–2 μm, reflected a paucity of very short intervals. A gap of at least 1 μm was indeed expected, because of the center-to-center measurement method and the $\approx$1-μm average length of varicosities. Second, interval variability was high, with roughly exponential interval distributions. Highly regular spacing, in contrast, would have given sigmoidally shaped distributions.

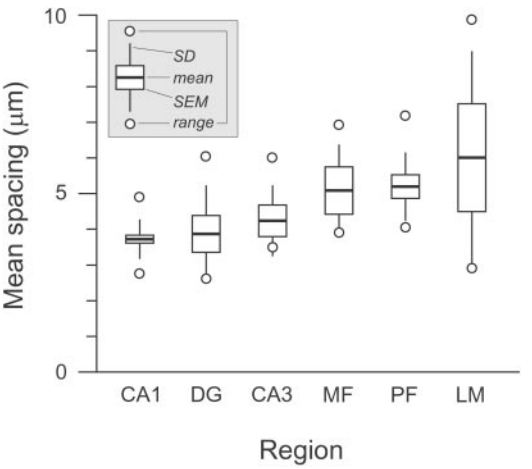

Fig. 3. Regional variability in mean varicosity spacing.

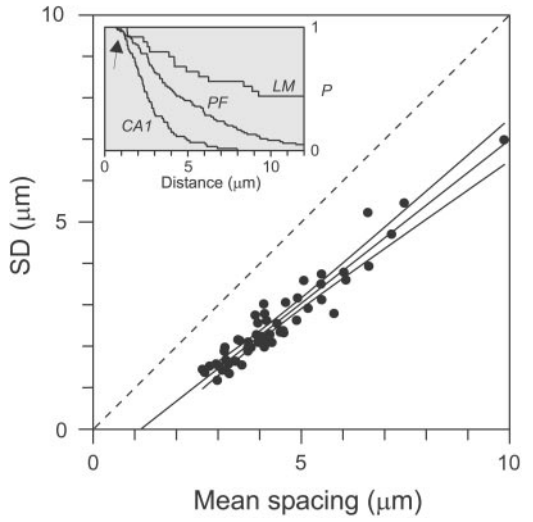

Fig. 4. Intervaricosity interval analysis. SD vs. mean spacing plotted for all axons. Identity line (dashed) with slope = 1 indicates Poisson relationship. Line through data, $y = 0.79x - 0.91$, was obtained by linear regression and extrapolated to the x axis. Also shown are the ±99% confidence intervals. (*Inset*) Representative interval distributions for three axons, including a PF and fibers in CA1 and LM, plotted as survival functions (inverse rank-ordered sets of intervals); for any distance in micrometers, P is the fraction of varicosities separated by at least that amount. Arrow points to gaps in distributions at shortest distances.

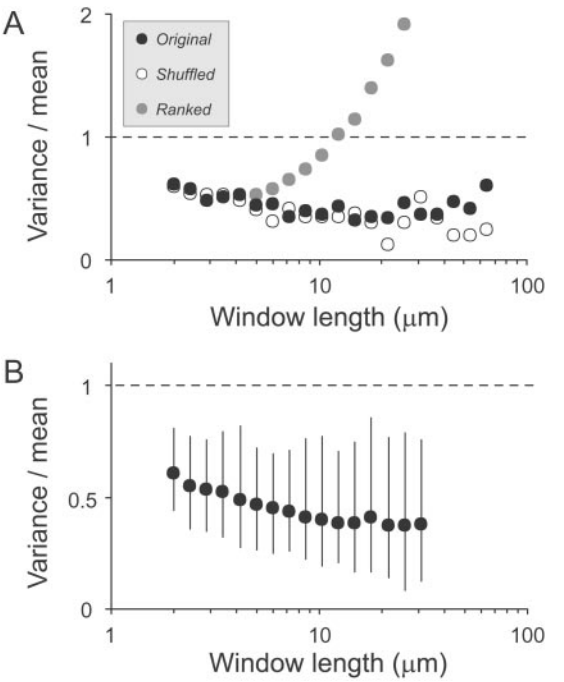

Fig. 5. Window analysis. (*A*) Index of dispersion (variance/mean) vs. window length, for a single axon (●). For comparison, the axon's sequence of the intervaricosity intervals was randomly shuffled (○) or ordered by rank (gray circles). (*B*) Overall averages of all axons' indices of dispersion, for different window lengths, shown with 5–95% confidence intervals.

The SD and mean of each axon's intervals, plotted in Fig. 4, were strongly correlated (Pearson's $r = 0.91$). Linear regression gave a line with a slope of 0.79 (99% confidence interval: 0.70–0.88), crossing the x axis at 1.2 μm. This relationship reveals two novel properties. It shows that the variability in varicosity spacing scales with the mean spacing, independent of axon type; axons apparently share a fundamentally similar varicosity distribution pattern despite average differences in varicosity spacing. It also clarifies the degree of randomness in varicosity spacing. The SD/mean ratio is the CV, a statistical estimator of variability whose value (and slope in the plot) is 1 if spacing is purely random (dashed identity line in Fig. 4) and 0 if perfectly regular. The data fall on a line whose slope was slightly but significantly (at a >99% confidence interval level) less than unity. The line appears right-shifted, by an amount similar to the gap in the interval distributions noted above. This "refractory distance" effect reduced the CVs to as low as 0.5 for the most densely varicose axons, akin to the regularizing effect of a refractory period on interspike intervals.

Are varicosities distributed evenly along axons, or organized into patterns? Although methods for interval analysis including auto- and serial correlation (data not shown; see also refs. 18, 24) did not detect obvious, repeated patterns, they could easily have missed gradients, clusters, and other heterogeneities. We therefore used window-based methods. For each axon we counted varicosities in consecutive windows, obtaining the variance and mean for different window lengths. The variance/mean ratio is the index of dispersion (Fano factor), a statistical estimator of homogeneity in event distributions. For a Poisson process it equals 1 for any window length; higher values reflect heterogeneity and lower values homogeneity. In the example of a single axon shown in Fig. 5*A* (●), indices were clearly below 1 and correlated negatively with window length for most window sizes, up to at least 20 μm (in this case values also trended upward for the longest windows). Rank-ordering the sequence of this axon's set of intervals demonstrated the maximal possible effect of heterogeneity; i.e., how high the indices could have been (gray circles). With this arrangement, an idealized gradient, values increased steeply above 1 for windows over 12 μm. Conversely, random shuffling of the sequence demonstrated the maximal possible effect of homogeneity; i.e., how low the indices could have been (○). This gave values closely resembling the original data. Thus, varicosities were homogeneously dispersed along this axon. Most axons gave similar results. As summarized in Fig. 5*B*, indices averaged well below 1 for all window lengths, were correlated negatively with window length (46/56 axons; $P < 10^{-5}$) and reached minimum values with windows greater than 10 μm. The axons' indices also correlated positively with their mean varicosity spacing (Pearson's $r = 0.4$), a reflection of the regularizing effect of the refractory distance on spacing. Finally, we attempted to detect subtle clustering, by simulating a large number of axons, with intervals identical to the originals in value but random in sequence, and comparing the *maximal* varicosity counts for each axon in the simulated and original groups (see *Materials and Methods*). The original axons differed significantly for 5-μm window ($P = 0.002$) but not other windows (7.5–85 μm). Thus, for these axons, clustering was a relatively weak effect detectable only at the population level. Lack of evidence for strong gradients or clusters here does not preclude their existence on longer scales. Indeed, proximodistal varicosity spacing gradients over millimeters have been reported for PFs (9); such gradients would have been mild (<10%) on the distances examined here.

Discussion

By comparing varicosity spacing along different types of central unmyelinated axons, we identified aspects of variability and reliability at several levels. On short scales, varicosity spacing was highly variable but not simply random. Similar patterns are evident in data from neocortical axons (18, 24, 25), hippocampal axons in culture (26), and corticostriatal axons (27). Hellwig *et al.* (18) noted that short-interval gaps reflect the finite lengths

of varicosities but emphasized the apparent randomness of varicosity distributions. Our data differ in showing clearly subrandom varicosity distributions. Their inference that synaptic distributions are random agrees with ours, but we reach this through a quantitative model relating varicosities and synapses (see below). Although the two studies differ in this detail, they otherwise broadly agree: our findings support their observations of spacing variability and show this to apply generally to a spectrum of axon types in different brain regions.

Previous estimates of varicosity spacing range widely (18, 24, 27–29), even for a single axon type such as CA3-to-CA1 axons or PFs (1, 2, 5, 9, 26, 30). Our results show that CA3-to-CA1 and PF axons have distinct, narrow ranges of mean spacing. This validates a useful connectivity rule: where axonal synaptic spacing is of a known and stereotypic value, the total number of synapses made by axons of that type can be predicted from their length. The regional differences also suggest that varicosity spacing is regulated, but at what level, and how? A related issue is whether axonal connectivity at different levels is probabilistic, deterministic, or a hybrid of both (discussed in ref. 18). In principal, varicosity spacing could be governed locally via a strong "relative" refractory distance; for instance, neighboring varicosities could "repel" one another. However, spacing would then tend to be either regular, if all varicosities repelled similarly, or correlated with varicosity size, if larger varicosities repelled more. A weak effect cannot be ruled out, however, and is compatible with the subrandom slope in the SD/mean relationship. Nor did we find substantial varicosity clustering, a candidate mechanism at the branch level; although clustering could provide spatial specificity in neural connections, so could other mechanisms such as regulating the number and length of branches to a target (18, 24, 31, 32). A mechanism not supported by our data are local bending of axon branches toward specific targets because branches were virtually straight.

A quantitative model relating synapses and varicosities should account for: (*i*) a synapse/varicosity ratio averaging slightly above 1 and varying in individual varicosities because of the occurrence of MSBs, (*ii*) variable varicosity spacing, with distributions marked by (*iii*) sub-Poisson CVs (Fig. 4) and (*iv*) sub-Poisson indices of dispersion (Fig. 5). A simple model fulfills these criteria, based on three plausible assumptions: that synapses are distributed randomly (or nearly so) along axons; that synapses are associated with varicosities (supported by evidence that an organelle carries an "obligatory volume" of cytoplasm; ref. 33); and that synapses closer together than a varicosity length generate varicosities that overlap, fusing into a larger MSB. Axons generated by this "varicosity fusion" model (Fig. 6*B*) gave varicosity data (solid symbols) that closely resembled the experimental results, including CVs (Fig. 6*D*) and indices of dispersion (Fig. 6*F*). A minor difference was the slightly subunity slope in the SD/mean relationship (Fig. 6*D*). The occurrence of MSBs gave an average synapse/varicosity ratio of 1.4. Synaptic data (open symbols in Fig. 6 *D* and *F*) were ≈1 in both plots because synaptic positions were random. An interesting property of this model is that MSB frequency depends inversely on mean varicosity spacing.

We also evaluated an alternative "varicosity fission" model (Fig. 6*C*), which relates to the suggestion, discussed below, that MSBs can split into single-synapse boutons (15, 16). In this model, MSBs are transient, being converted to single-synapse varicosities by increasing the separation between any too-close synapses. Because all varicosities end up with exactly one synapse, synaptic and varicosity distributions are identical. Axons generated by this model gave data that clearly differed from the original data (Fig. 6 *E* and *G*). Although the final axons produced by this model do not fulfill the criterion of >1 synapse/varicosity ratio, the initial ones do; moreover, similar results were obtained even if several percentage of MSBs were left intact.

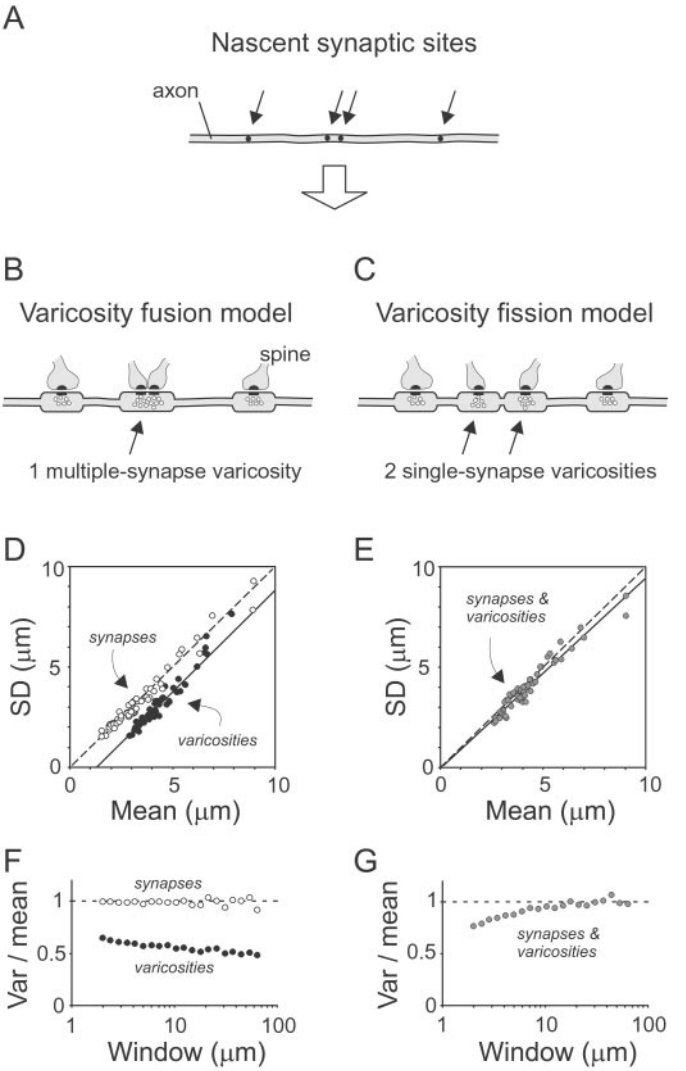

Fig. 6. Models of synapse-varicosity relationships. (*A*) Positions (arrows) along an axon where synapses and subsequently varicosities will form. (*B* and *C*) Two models of how varicosities form near synapses. In the varicosity fusion model, varicosities 1.0 μm in length form around every synapse. If two synapses are closer than the varicosity length, their varicosities are fused into one longer varicosity, creating a MSB. In the varicosity fission model, MSBs are converted into two single-synapse boutons by sliding synapses apart. (*D* and *E*) SD vs. mean spacing for axons simulated according to the two models. (*F* and *G*) Indices of dispersion for simulated axons. ●, Varicosity data; ○, synaptic data; and gray circles, overlapping synaptic and varicosity data.

Synaptogenesis at CA3-to-CA1 synapses is associated with an increased frequency of MSBs (12–14, 17). Views differ on the fate of MSBs. In one, compatible with the fusion model and with evidence that new synapses arise at existing boutons, MSBs are stable (12, 13, 17, 34, 35). In another, compatible with the fission model, MSBs divide to form single-synapse boutons (15, 16), a process reported for invertebrate motor terminals (36, 37). Our results make fission unlikely as a major mechanism for varicosity formation along vertebrate central axons, although a role in plasticity at a subset of synapses is possible. Space limitations further constrain models involving varicosity neogenesis (19) because the presence of existing varicosities and of very short intervaricosity intervals would render a sizeable fraction of an unmyelinated axon's length "refractory" to new varicosities—estimated at nearly 60% for the most varicose axons in this study. Taken together, the statistical estimators of variability quantified

here place limits on where and how many new varicosities can arise along axons before falling outside the population (i.e., varicosity spacing is a "stiff" system) and provide a framework for detecting changes in axonal varicosity distributions under dynamic conditions such as development and plasticity.

We thank Johannes Helm and Finn Mogens Haug for sharing expertise and facilities, and Mitya Chklovskii, Kristen Harris, Vidar Jensen, and Armen Stepanyants for useful discussions. This work was supported by the Norwegian Research Council (P.A.) and a Human Frontiers Science Program Organization fellowship (to G.M.G.S.).

1. Ishizuka, N., Weber, J. & Amaral, D. G. (1990) *J. Comp. Neurol.* **295,** 580–623.
2. Li, X. G., Somogyi, P., Ylinen, A. & Buzsáki, G. (1994) *J. Comp. Neurol.* **339,** 181–208.
3. Westrum, L. E. & Blackstad, T. W. (1962) *J. Comp. Neurol.* **119,** 281–309.
4. Napper, R. M. A. & Harvey, R. J. (1988) *J. Comp. Neurol.* **274,** 168–177.
5. Shepherd, G. M. G. & Harris, K. M. (1998) *J. Neurosci.* **18,** 8300–8310.
6. Harris, K. M. & Stevens, J. K. (1988) *J. Neurosci.* **8,** 4455–4469.
7. Harris, K. M. & Stevens, J. K. (1989) *J. Neurosci.* **9,** 2982–2997.
8. Sorra, K. E. & Harris, K. M. (1993) *J. Neurosci.* **13,** 3736–3748.
9. Pitchitpornchai, C., Rawson, J. A. & Rees, S. (1994) *J. Comp. Neurol.* **342,** 206–220.
10. Schikorski, T. & Stevens, C. F. (1997) *J. Neurosci.* **17,** 5858–5867.
11. Anderson, J. C., Binzegger, T., Martin, K. A. C. & Rockland, K. S. (1998) *J. Neurosci.* **18,** 10525–10540.
12. Woolley, C. S., Wenzel, H. J. & Schwartzkroin, P. A. (1996) *J. Comp. Neurol.* **373,** 108–117.
13. Kirov, S. A., Sorra, K. E. & Harris, K. M. (1999) *J. Neurosci.* **19,** 2876–2886.
14. Toni, N., Buchs, P.-A., Nikonenko, I., Bron, C. R. & Muller, D. (1999) *Nature (London)* **402,** 421–425.
15. Lüscher, C., Nicoll, R. A., Malenka, R. C. & Muller, D. (2000) *Nat. Neurosci.* **3,** 545–550.
16. Muller, D., Toni, N. & Buchs, P.-A. (2000) *Hippocampus* **10,** 596–604.
17. Yankova, M., Hart, S. & Woolley, C. S. (2001) *Proc. Natl. Acad. Sci. USA* **98,** 3525–3530.
18. Hellwig, B., Schüz, A. & Aertsen, A. (1994) *Biol. Cybern.* **71,** 1–12.
19. Bozdagi, O., Shan, W., Tanaka, H., Benson, D. L. & Huntley, G. W. (2000) *Neuron* **28,** 245–259.
20. Kirov, S. A. & Harris, K. M. (1999) *Nat. Neurosci.* **2,** 878–883.
21. Perkel, D. H., Gerstein, G. L. & Moore, G. P. (1967) *Biophys. J.* **7,** 391–440.
22. Ramón y Cajal, S. (1911) *Histologie de Système Nerveux de l'Homme et des Vertébrés* (Maloine, Paris), Vol. 2.
23. Acsády, L., Kamondi, A., Sík, A., Freund, T. & Buzsáki, G. (1998) *J. Neurosci.* **18,** 3386–3403.
24. Amir, Y., Harel, M. & Malach, R. (1993) *J. Comp. Neurol.* **334,** 19–46.
25. Martin, K. A. C. & Whitteridge, D. (1984) *J. Physiol.* **353,** 463–504.
26. Forti, L., Bossi, M., Bergamaschi, A., Villa, A. & Malgaroli, A. (1997) *Nature (London)* **388,** 874–878.
27. Kincaid, A. E., Zhengh, T. & Wilson, C. J. (1998) *J. Neurosci.* **18,** 4722–4731.
28. Lübke, J., Egger, V., Sakmann, B. & Feldmeyer, D. (2000) *J. Neurosci.* **20,** 5300–5311.
29. Weller, R. E., White, D. M. & Walton, M. M. G. (2000) *J. Comp. Neurol.* **420,** 52–69.
30. Andersen, P., Trommald, M. & Jensen, V. (1994) in *Molecular and Cellular Mechanisms of Neurotransmitter Release*, eds. Stjärne, L., Greengard, P., Grillner, S., Hökfelt, T. & Ottoson, D. (Raven, New York), pp. 341–351.
31. Shatz, C. J. & Stryker, M. P. (1978) *J. Physiol. (London)* **281,** 267–283.
32. de Bello, W. M., Feldman, D. E. & Knudsen, E. I. (2001) *J. Neurosci.* **21,** 3161–3174.
33. Sasaki-Sherrington, S. E., Jacobs, J. R. & Stevens, J. K. (1984) *J. Cell. Biol.* **98,** 1279–1290.
34. Geinisman, Y., Berry, R. W., Disterhoft, J. F., Power, J. M. & van der Zee, E. A. (2001) *J. Neurosci.* **21,** 5568–5573.
35. Ma, L., Zablow, L., Kandel, E. R. & Siegelbaum, S. A. (1999) *Nat. Neurosci.* **2,** 24–30.
36. Zito, K., Parnas, D., Fetter, R. D., Isacoff, E. Y. & Goodman, C. S. (1999) *Neuron* **22,** 719–729.
37. Roos, J., Hummel, T., Ng, N., Klämbt, C. & Davis, G. W. (2000) *Neuron* **26,** 371–382.